Flexible graphene-based lithium ion batteries with ultrafast charge and discharge rates

Na Li[a,b,1], Zongping Chen[a,1], Wencai Ren[a], Feng Li[a], and Hui-Ming Cheng[a,2]

[a]Shenyang National Laboratory for Materials Science, Institute of Metal Research, Chinese Academy of Sciences, Shenyang 110016, China; and [b]Department of Materials Science & Engineering, School of Chemistry and Materials Science, University of Science and Technology of China, Hefei 230026, China

Edited* by Mildred S. Dresselhaus, Massachusetts Institute of Technology, Cambridge, MA 02139 and approved September 17, 2012 (received for review June 13, 2012)

There is growing interest in thin, lightweight, and flexible energy storage devices to meet the special needs for next-generation, high-performance, flexible electronics. Here we report a thin, lightweight, and flexible lithium ion battery made from graphene foam, a three-dimensional, flexible, and conductive interconnected network, as a current collector, loaded with $Li_4Ti_5O_{12}$ and $LiFePO_4$, for use as anode and cathode, respectively. No metal current collectors, conducting additives, or binders are used. The excellent electrical conductivity and pore structure of the hybrid electrodes enable rapid electron and ion transport. For example, the $Li_4Ti_5O_{12}$/graphene foam electrode shows a high rate up to 200 C, equivalent to a full discharge in 18 s. Using them, we demonstrate a thin, lightweight, and flexible full lithium ion battery with a high-rate performance and energy density that can be repeatedly bent to a radius of 5 mm without structural failure and performance loss.

flexible device | full battery

The development of next-generation flexible electronics (1), such as soft, portable electronic products, roll-up displays, wearable devices, implantable biomedical devices, and conformable health-monitoring electronic skin, requires power sources that are flexible (2, 3). Similar to conventional energy storage devices, flexible power sources with high capacity and rate performance that enable electronic devices to be continuously used for a long time and fully charged in a very short time are very important for applications of high-performance flexible electronics (4–7). Lithium ion batteries (LIBs) have a high capacity but usually suffer from a low charge/discharge rate compared with another important electrochemical storage device, supercapacitors. Therefore, it is highly desired to fabricate a flexible electrochemical energy storage system with a supercapacitor-like fast charge/discharge rate and battery-like high capacity. However, the fabrication of such an energy storage device remains a great challenge owing to the lack of reliable materials that combine superior electron and ion conductivity, robust mechanical flexibility, and excellent corrosion resistance in electrochemical environments.

Using nano-sized materials to prepare electrodes is one of the most promising routes toward flexible batteries. Metal oxide nanowires (8, 9) and carbon nanomaterials such as carbon nanotubes (6, 10–12) and graphene paper (13) have been recently demonstrated for use in flexible LIBs. However, electron transport in these electrodes is slow because of the relatively low quality of nanomaterials (such as chemically derived graphene) and/or high junction contact resistance between them. As a consequence, only a moderate charge/discharge rate has been obtained in these flexible batteries. It is generally believed that the charge/discharge rate of a LIB depends critically on the migration rate of lithium ions and electrons through the electrolyte and bulk electrodes into active electrode materials. Strategies to increase ion and electron transport kinetics in batteries have mainly focused on seeking new electrode materials and designing conductive electrode structures with high ion and electron transport rates (4, 5, 14, 15), or reducing the path length over which electrons and lithium ions have to move by using nanomaterials (16–18). Based on these strategies, electrodes with a highly conductive pathway for electrons, a short ion diffusion length, and a fast transport channel for the ion flux can be fabricated for fast charge and discharge. A series of electrochemical active materials (4, 15–18) and three-dimensional (3D) hybrid electrodes (5, 14) have been recently fabricated to assemble rechargeable batteries with high charge and discharge rates. For example, Braun et al. (5) recently fabricated a macroporous nickel network for battery electrodes with ultrafast charge and discharge rates, and 76% of the specific capacity was retained when discharged at 185 C. However, these batteries are based on a complicated electrode package and rigid electrode structures with metals as current collectors, which makes the devices less flexible, and they also have a low energy density.

Recently, we have fabricated a unique 3D graphene macroscopic structure: graphene foam (GF) (19). A GF consisting of a 3D interconnected network of high-quality chemical vapor deposition-grown graphene can be used as the fast transport channel of charge carriers. The electrical conductivity of the GF is estimated as high as ~1,000 S/m, and the solid conductivity of the few-layer graphene itself within the GF is evaluated to be $\sim 1.36 \times 10^6$ S/m (*SI Appendix*). Moreover, the GF is extremely light (~0.1 mg/cm^2 with a thickness of ~100 μm) and flexible. It possesses a high porosity of ~99.7% and a very high specific surface area and can be bent to arbitrary shapes without breaking. In addition, the high quality and carbonaceous nature of graphene building blocks give the GF network excellent stability in electrochemical environments. These features give the GF great potential for use in next-generation flexible electronics. Using the GF network as both a highly conductive pathway for electrons and ions and a 3D interconnected current collector, we have developed thin, lightweight, and flexible $LiFePO_4$ (LFP)/GF and $Li_4Ti_5O_{12}$ (LTO)/GF electrodes that can simultaneously obtain high charge and discharge rates up to 200 C (where a 1-C rate represents a 1-h complete charge or discharge). Using these flexible bulk electrodes, we further assembled a thin, lightweight, and flexible full LIB (Fig. 1) that shows high capacity and high-rate performance and is capable of repeated bending to a radius of <5 mm without structural failure and loss of performance.

Results and Discussion

Synthesis and Characterization of Free-Standing Flexible LTO/GF and LFP/GF. LTO and LFP have been considered as promising anode and cathode materials for commercial applications in LIBs because of their safety, environmental friendliness, and high

Author contributions: N.L., Z.C., W.R., F.L., and H.-M.C. designed research; N.L. and Z.C. performed research; N.L., Z.C., W.R., F.L., and H.-M.C. analyzed data; and N.L., Z.C., W.R., F.L., and H.-M.C. wrote the paper.

The authors declare no conflict of interest.

*This Direct Submission article had a prearranged editor.

[1]N.L. and Z.C. contributed equally to this work.

[2]To whom correspondence should be addressed. E-mail: cheng@imr.ac.cn.

This article contains supporting information online at www.pnas.org/lookup/suppl/doi:10.1073/pnas.1210072109/-/DCSupplemental.

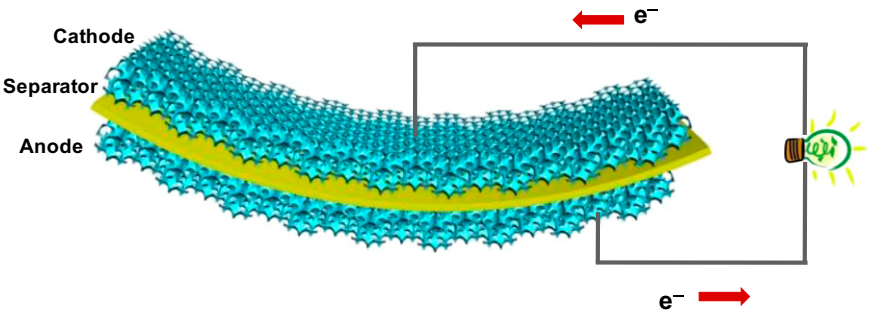

Fig. 1. Schematic of a flexible battery containing a cathode and an anode made from 3D interconnected GF.

performance. To build a flexible LIB with a high capacity and fast charge and discharge rates, we integrated highly conductive, porous, and flexible GF with LTO and LFP as anode and cathode, respectively (Fig. 1). It is worth noting that the 3D porous GF network was directly used as a highly conductive pathway for electrons/lithium ions and current collectors for the LIB, without the use of conventional metal current collectors, carbon black additive and binder. The LTO/GF and LFP/GF hybrid materials were fabricated by in situ hydrothermal deposition of active materials on GF followed by heating in an argon atmosphere (details in *Methods* and *SI Appendix*). Notably, similar to GF, these hybrid materials are very flexible (Fig. 2*A*), can be bent into arbitrary shapes without breaking, and completely preserve the 3D interconnected network structure of the GF (Fig. 2*B*).

The LTO in the hybrid material has a sheet structure a few nanometers in thickness, and high-density LTO sheets stand perpendicular to the surface of the GF, which not only provides a large interfacial area for fast lithium insertion/extraction but also ensures a short solid-state diffusion length (Fig. 2 *C* and *D* and *SI Appendix*, Fig. S1). The LTO sheet growth is nucleated at wrinkles on the GF because of their higher chemical reactivity (*SI Appendix*). The direct growth of LTO on the GF enables good contact and strong binding between LTO and GF, with no need to add any binder. As a result, no LTO nanosheets were peeled off even after repeated bending (*SI Appendix*, Fig. S2). The transmission electron microscope (TEM) image (Fig. 2*E*) shows that the LTO nanosheets are several hundred nanometers in width and a few nanometers in thickness. The high-resolution TEM image in Fig. 2*F* indicates the high crystallinity of the nanosheets with a lattice fringe spacing of 4.8 Å, corresponding to the most stable and frequently observed (111) facet of spinel LTO (*SI Appendix*, Fig. S3), which is consistent with the X-ray

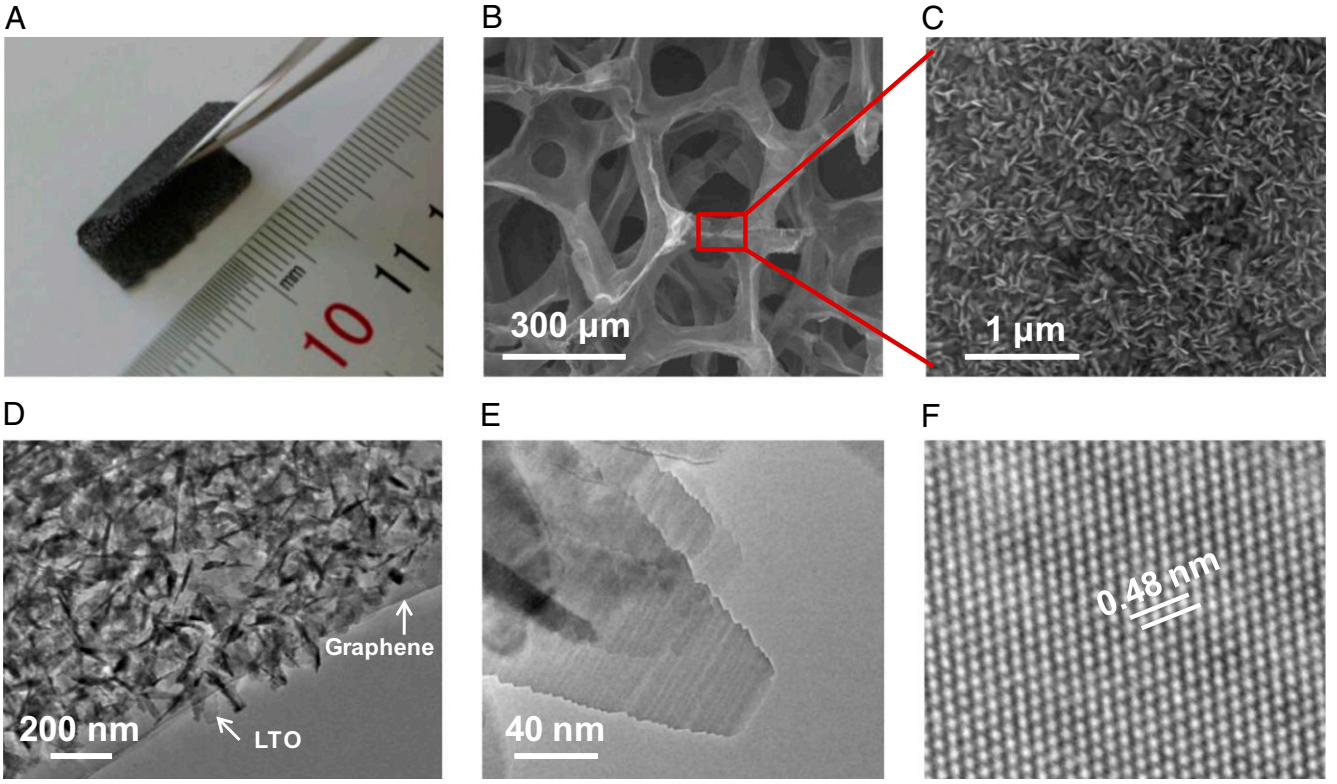

Fig. 2. Characterization of a free-standing flexible LTO/GF. (*A*) Photograph of a free-standing flexible LTO/GF being bent (2×2 cm^2). (*B* and *C*) SEM images of the LTO/GF. (*D*) TEM image of the LTO/GF. (*E*) TEM image of the LTO nanosheets in LTO/GF. (*F*) High-resolution TEM image of a LTO nanosheet showing lattice fringes with a spacing of 0.48 nm.

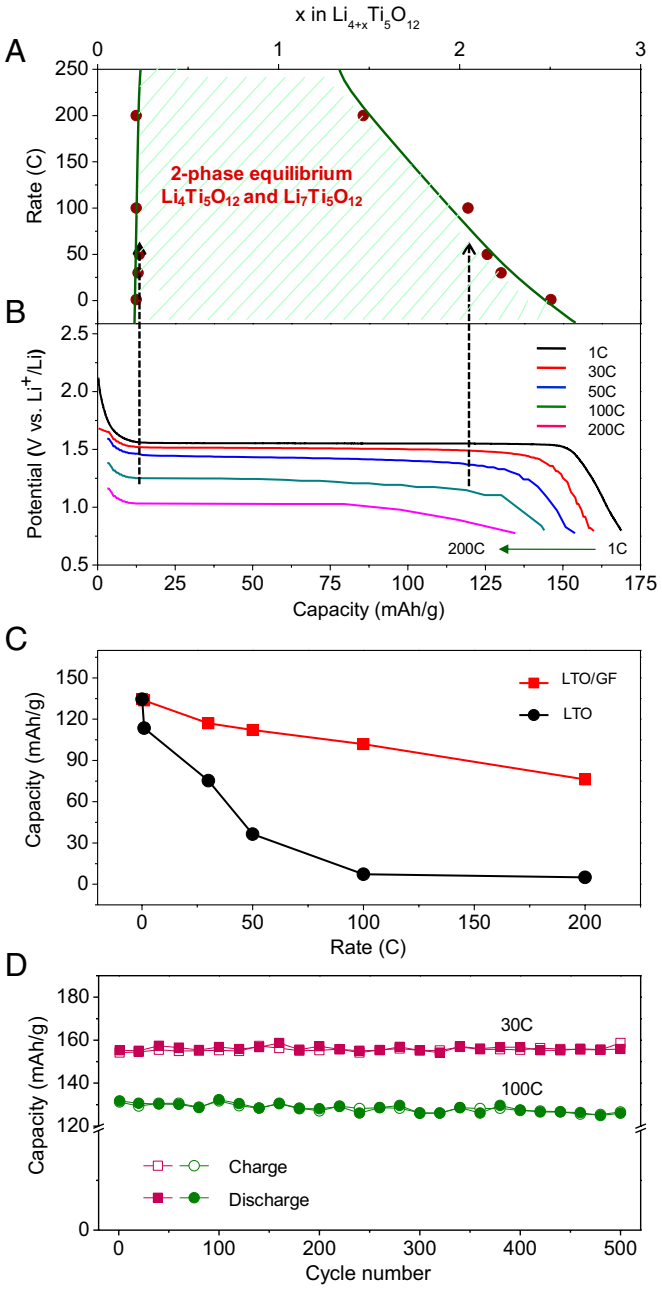

Fig. 3. Discharge rate and cyclic performance of the LTO/GF electrode. (*A*) Two-phase equilibrium region of the LTO/GF with different charge/discharge rates; C/*n* denotes the rate at which a full charge or discharge takes *n* hours. (*B*) Discharging voltage curves of the LTO/GF with different charge/discharge rates. (*C*) Specific capacities of the LTO/GF and reference LTO at various charge/discharge rates within a flat plateau segment shown in *B*. (*D*) Capacities of the LTO/GF charged/discharged at constant 30-C and 100-C rates for 500 cycles.

diffraction measurements (JCPDS 49–0207; *SI Appendix*, Fig. S4*A*). In addition, similar to the pristine GF (19), the Raman spectra of a free-standing LTO/GF material shows a strongly suppressed defect-related D band (*SI Appendix*, Fig. S5), indicating the overall high quality of graphene in LTO/GF. This also suggests that no defects were introduced in GF during the LTO synthesis process, guaranteeing a very high electrical conductivity of the GF. The above features of this 3D porous LTO/GF hybrid electrode produce a highly conductive pathway for electrons, a short ion diffusion length, and a fast transport channel for a high Li^+ flux, which provide the electrodes with a great potential for fast charge and discharge.

Electrochemical Behavior of the LTO/GF Anode. We investigated the lithium insertion/extraction properties of the LTO/GF material by galvanostatic charge–discharge measurements (Fig. 3) and found that this LTO/GF hybrid material shows extremely high charge/discharge rates. At a charge/discharge rate of 0.1 C, the LTO/GF and LTO have similar specific charge/discharge capacities. However, at charge/discharge rates of 1 C and 30 C, the LTO/GF shows a specific capacity of about 170 and 160 mAh/g, respectively, and even at a charge and discharge rate of 200 C (corresponding to an 18-s full discharge), it still retains a specific capacity of 135 mAh/g, corresponding to ∼80% of the specific capacity at the 1-C rate. In contrast, the reference LTO, which was prepared using the same process but without the presence of GF, shows a capacity of almost zero at 200 C, although it also has a 2D sheet structure (*SI Appendix*, Fig. S6). Moreover, the rate performance of this LTO/GF material is much better than those reported in the literature for all kinds of conventional LTO electrodes integrated with metal foil current collectors, carbon black additive and binder, including nanocrystalline LTO, carbon-coated LTO, and LTO/multiwalled carbon nanotube and LTO/graphene composites (*SI Appendix*, Table S1). To further determine the stability of the electrode structure, we studied the change in morphology of the LTO/GF electrode after 100 charge/discharge cycles at 0.5 C and found that the LTO/GF electrode is capable of long-term lithiation and delithiation at low rates without structural failure (*SI Appendix*, Fig. S7).

More strikingly, the discharge curve of the LTO/GF anode at high rates (up to 200 C) shows a long, flat potential plateau, which ensures a constant power output, and therefore is very important for the commercial use of LIBs (20). The flat plateau segment is a characteristic of two-phase equilibrium (21), a room-temperature miscibility gap, as shown in Fig. 3*A*. In contrast, although many nanostructured materials have been developed to show high-rate performance (4, 5, 22–24), most of them exhibit a nonflat plateau with a capacitor-like charge–discharge curve at high rates. The profile change of voltage curves from flat to slope at high rates may be attributed to polarization related to the poor electrical conductivity of electrode materials, or may occur because electrode materials obey a pseudocapacitive (interfacial) storage mechanism instead of a bulk intercalation storage mechanism (25). The high-rate performance with a long, flat plateau in the potential profile of the LTO/GF electrode suggests excellent ion and electron transport kinetics of the LTO/GF hybrid structure. As shown in Fig. 3*C*, the specific capacity of the flat plateau segment of the LTO/GF at 200 C is 86 mAh/g, whereas the value of the reference LTO is almost zero. Fig. 3*D* shows the cyclic stability of the LTO/GF at 30 C and 100 C. Note that the capacity decreases less than 4% of the initial value after 500 cycles, demonstrating the excellent electrochemical stability of this free-standing flexible electrode.

In general, in a commercial LIB, metal current collectors (mainly copper, ∼10 mg/cm^2 and aluminum, ∼5 mg/cm^2, with a thickness of ∼10–30 μm), conducting additives, and binding agents are indispensable, and these account for 30–50% of the electrode weight. Bulk electrodes constructed of either metal (5, 14) or pyrolytic carbon (26) have recently been developed for fast charge and discharge, but metal current collectors are still needed for facilitating electron transport from the electrode to the cell. These metal and carbonaceous components of bulk electrodes make a battery cell heavy and nonflexible. In contrast, in our electrode, the 3D flexible and conductive interconnected GF network acts not only as a highly conductive pathway for electrons/lithium ions but also as an ultralight current collector (down to ∼0.1 mg/cm^2) (*SI Appendix*, Fig. S8 *A* and *B*), without

the use of conductive additives, binding agents, and metal current collectors. Impedance spectroscopy was used to characterize the contact and charge-transfer resistance of the free-standing LTO/GF electrode (*SI Appendix*, Fig. S8*C*). The values of the contact resistance R_s and charge-transfer resistance R_{ct} of the LTO/GF electrode were 6.6 and 67.1 Ω, respectively, which are significantly lower than those of the reference LTO coated on an aluminum current collector (11.7 and 112.1 Ω) (*SI Appendix*, Table S2). These results confirm that the GF could not only preserve the high conductivity of the overall electrode, but also largely improve the electrochemical activity of LTO during the charge/discharge processes.

Electrochemical Behavior of the LFP/GF Cathode. To assemble a full LIB, we also fabricated a LFP/GF cathode, using a similar process for LTO/GF fabrication, to match the LTO/GF anode (*SI Appendix*, Figs. S4*B* and S9). Similar to the LTO/GF anode, this LFP/GF cathode is very flexible and shows excellent cyclic stability at both a low rate of 0.5 C and a high rate of 10 C (*SI Appendix*, Figs. S10 and S11), which further proves the importance of the 3D conductive interconnected GF network, as well as the good contact and strong binding between LFP and the GF. The specific capacity of the LFP/GF electrode at a 50-C discharge rate is 98 mAh/g (*SI Appendix*, Fig. S11*A*), which is higher than those of LFP/chemically derived graphene hybrid electrodes integrated with aluminum foil current collectors, carbon black additive, and binder (27, 28). This high-rate performance is much better than that of a flexible LFP/multiwalled carbon nanotube-yarn electrode, which only retained a capacity of ∼50 mAh/g at a 10-C rate (12). Furthermore, at a 10-C charge/discharge rate, 98% capacity retention was obtained after 500 cycles for the LFP/GF electrode (*SI Appendix*, Fig. S11*B*). It should be pointed out that Huang and coworkers (29) recently used a graphene network to improve the rate performance of a LFP cathode. Different from our preparation process, their LFP/graphene network material was prepared by simply mixing a graphene network with a suspension of LFP powder by stirring. Moreover, a poly (vinyl difluoride) binder and acetylene black were used in the fabrication of the LFP/graphene network electrode by magnetic stirring. This LFP/graphene electrode showed a moderate-rate performance similar to LFP/chemically derived graphene electrodes (27, 28), possibly because the graphene conductive network may be broken during the stirring process, resulting in damage to the unique structure and degradation in the properties of the GFs.

It is worth pointing out that the charge/discharge curve of the pristine GF (*SI Appendix*, Fig. S12) shows a long, flat potential plateau at about 0.2 V, which means that lithium ions can

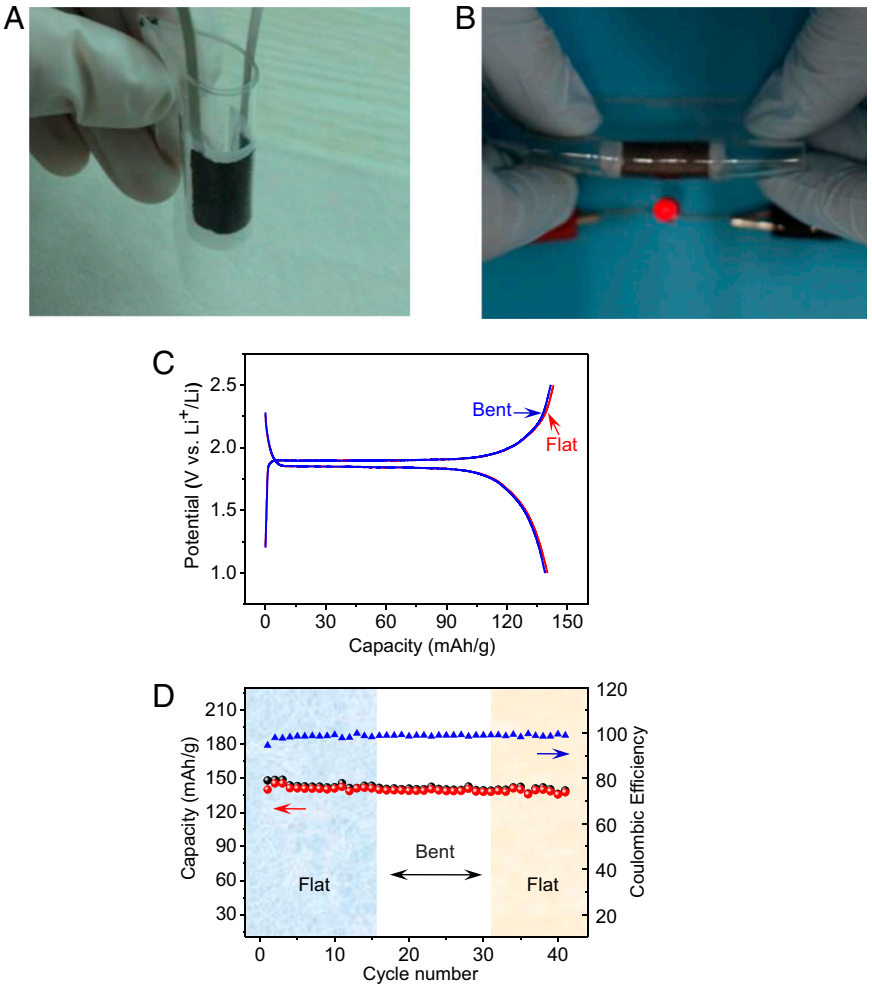

Fig. 4. Characterization of a thin, lightweight, and flexible LTO/GF//LFP/GF full battery. (*A*) Photograph of a bent battery encapsulated by PDMS, showing its good flexibility. (*B*) Lighting a red LED device under bending. (*C*) Galvanostatic charging/discharging curves of the battery. Red and blue lines represent the as-fabricated flat battery and the bent battery after repeatedly bending to a radius of 5 mm 20 times, respectively. (*D*) Cyclic performance of the battery under flat and bent states.

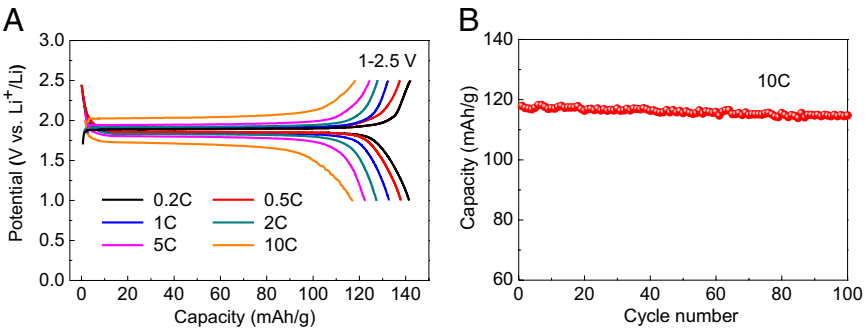

Fig. 5. Rate and cyclic performance of a flexible LTO/GF//LFP/GF full battery. (*A*) Charging/discharging voltage curves of the battery with different current rates. (*B*) Capacity of the battery charged/discharged at a constant 10-C rate for 100 cycles.

intercalate into GF below 0.2 V. However, the voltage windows used for the LTO/GF and LFP/GF in this work are 0.8–2.5 V and 2.5–4.2 V, respectively. Therefore, these high-voltage windows prevent lithium intercalation in GF.

Assembling and Electrochemical Behavior of a Flexible Full Battery. The voltage profiles of the LTO/GF and LFP/GF electrodes were investigated before assembling a full battery (*SI Appendix*, Fig. S13), and no significant overpotential was observed. The LTO/GF and LFP/GF electrodes showed initial discharge capacities of 170 mAh/g and 164 mAh/g at 0.2 C, respectively. These results indicate that the LTO/GF is a good match with the LFP/GF for assembling a full battery. Using the flexible LFP/GF cathode and LTO/GF anode, we then built a thin, lightweight, and flexible LTO/GF//LFP/GF full battery. The free-standing LTO/GF and LFP/GF electrodes with a thickness of ∼100 μm were first laminated onto both sides of a polypropylene separator and then sealed with ∼250-μm-thick poly (dimethyl siloxane) (PDMS) in an Ar-filled glove box using $LiPF_6$ in ethylene carbonate/dimethyl carbonate as the electrolyte. The total thickness of this flexible full battery is less than 800 μm. Due to the small thickness and great flexibility of the GF-based electrodes (Fig. 2*A*), the full battery shows excellent flexibility, and no structural failure was observed after repeatedly bending to a radius of <5 mm (Fig. 4*A*). This flexible battery is able to power a red light-emitting diode (LED) when bent, as shown in Fig. 4*B*. As expected from the operating voltages of the LTO/GF and LFP/GF, their combination produces a battery with an operating voltage of 1.9 V, and the initial discharge capacity of the battery is ∼143 mAh/g with a Coulombic efficiency of 98% at a 0.2-C rate (Fig. 4*C*). In this full battery, all of the inactive components (metal current collectors, conducting additives, and binders) are replaced by lightweight GF (nearly two orders of magnitude lighter in areal density and three orders of magnitude lighter in volume density than copper); our flexible battery shows an energy density of ∼110 Wh/kg based on the total mass of the LTO/GF anode and LFP/GF cathode. A higher energy density can be obtained by using materials with a wider voltage window. Although the volume energy density of the LTO/GF//LFP/GF battery is not very high at low discharge rates, it becomes very good at high discharge rates compared with the batteries not using GF, and it is possible to increase its energy density. For example, the volume energy density of the battery can be increased by increasing the thickness of active materials, improving the assembly process, selecting better packaging materials, and controlling the thickness of the GF used. To further increase the volume energy density of a flexible battery, one can deposit electrochemically active materials with extremely high energy density, such as metal oxides and silicon.

We also investigated the effect of bending on the performance of the flexible battery. After 20 bends to a radius of 5 mm, only a negligible overpotential was observed, and the capacity of the battery being bent decreased less than 1% compared with that of the original flat battery (Fig. 4*C*). Moreover, the flexible battery showed an excellent cyclic stability both under flat and bent states. For example, with respect to the original capacity, the flexible battery showed a capacity retention of ∼97% after the first 15 cycles under a flat state, and ∼95% after another 15 cycles under a bent state (a bend radius of 5 mm) (Fig. 4*D*).

The high-rate performance of the flexible battery was further investigated. Fig. 5 shows the insertion/extraction capacity of a flexible battery tested at different charge/discharge rates. It should be noted that the rate capability of a LTO/LFP full battery is limited by the cathode material, and it is lower than that of a half cell (*SI Appendix*, Table S3). This flexible full battery can be operated at a 10-C rate with a capacity of 117 mAh/g (Fig. 5*A*), 88% of the capacity at a 1-C rate, which surpasses most full batteries reported (30–32) despite the fact that they are all based on a conventional, nonflexible electrode package integrated with metal foil current collectors, carbon black additive, and binder, because the fast charge/discharge performance of a flexible full battery has never been reported (6, 11, 13). Furthermore, our flexible full battery can be cycled over 100 cycles at a high rate of 10 C with only 4% capacity loss (Fig. 5*B*). Such a high-rate, long-life performance for this flexible LTO/GF//LFP/GF battery, to our knowledge, has never been reached before.

Conclusion

In this work, we have demonstrated a thin, lightweight, and flexible LIB using a 3D flexible and conductive interconnected GF network as both a highly conductive pathway for electrons/lithium ions and light current collector. By using the flexible LTO/GF and LFP/GF as anode and cathode, respectively, a flexible full battery was assembled. This battery has shown good flexibility, high capacity, high rate, and long-life cyclic performance even under repeated bending to a small radius of 5 mm. Our strategy is versatile and can be used to fabricate a broad class of anode and cathode materials. Both the fabrication of GF and subsequent filling and loading of active materials can be easily scaled up, which opens up the possibility for large-scale fabrication of flexible batteries with high capacity to power flexible electronic devices that can be operated at a high power rate and fully charged in a very short time.

Methods

Synthesis of LTO/GF. The GF was prepared as previously reported (19). LTO/GF was prepared as follows. Typically, 1.7 mL of 30% (wt/wt) hydrogen peroxide was dispersed in 40 mL of 0.4 M LiOH, followed by the addition of 3 mmol of titanium tetraisopropoxide [Ti-$(OC_3H_7)_4$]. After stirring for 1 h, a piece of GF was soaked in the solution, which was then transferred to an 80-mL Teflon-lined stainless autoclave and held at 130 °C for 3–12 h before cooling to room temperature. The GF loaded with LTO nanosheets was washed with deionized water and dried in an oven at 80 °C. Finally, the as-prepared sample was heated in a muffle furnace at 550 °C for 6 h in argon. Reference

LTO powder was prepared under the same conditions but without the addition of GF to the reaction solution.

Synthesis of LFP/GF. In a typical synthesis process (33), 0.01 mol of lithium acetate hydrate ($CH_3COOLi{\cdot}2H_2O$), iron(III) nitrate hydrate ($Fe(NO_3)_3{\cdot}9H_2O$), and ammonium dihydrogen phosphate ($NH_4H_2PO_4$) were dissolved in 35 mL of distilled water; 2.5 mL of ethylene glycol was then added to the solution, and a yellow suspension was obtained. A piece of GF was soaked in this solution before being transferred to an 80-mL Teflon-lined autoclave. The autoclave was sealed, kept at 180 °C for 6 h, and then cooled to room temperature. The GF covered with LFP nanoparticles was washed with deionized water and dried in an oven at 80 °C. Finally, the as-prepared sample was heated at 720 °C for 12 h under a hydrogen and argon (5:95 vol/vol) atmosphere.

The graphene content in LTO/GF and LFP/GF hybrid materials was estimated to be ~12 wt%.

Characterization. XRD patterns of samples were recorded on a Rigaku diffractometer using Cu Kα irradiation. SEM and TEM images were obtained on a FEI Nova NanoSEM 430 and Tecnai F20, respectively. Raman measurements were performed on Jobin-Yvon LabRam HR 800 excited by a 632.8-nm laser.

Electrochemical Measurements. For half cell tests of free-standing LTO/GF and LFP/GF, coin cells were fabricated. In both cases, a lithium metal foil was used as the counter electrode, 1 M $LiPF_6$ in ethylene carbonate and dimethyl carbonate (1:1, vol/vol) as electrolyte, and Celgard 2400 polypropylene as separator. The charge/discharge cycles were performed at different rates at room temperature. All tests on the free-standing LTO/GF and LFP/GF were performed without conventional metal current collectors, carbon black and binder. The reference LTO electrode was prepared by mixing the pure LTO powder, carbon black (TIMCAL Super-P), and poly(vinyl difluoride) at a weight ratio of 80:10:10. The mixture was pasted onto a pure aluminum foil and then pressed and dried under vacuum at 120 °C for 12 h. Batteries were assembled in an argon-filled glove box with oxygen and water contents below 1 and 0.1 ppm, respectively. All of the capacities and C-rate currents in this work were calculated based on LTO and LFP active materials (1 C corresponding to 175 mA/g and 170 mA/g for LTO and LFP, respectively). For the full battery, the capacities and C-rate currents were calculated based on the cathode active material (1 C corresponding to 145 mA/g).

PDMS gel was fabricated by vigorously mixing base/curing agents (Sylgard 184; Dow Corning), followed by degassing in a vacuum oven for 30 min and thermally curing at 80 °C for 4 h.

ACKNOWLEDGMENTS. This work was supported by Ministry of Science and Technology of China Grant 2012AA030303, National Natural Science Foundation of China Grants 51172240, 50921004, and 50972147, and Chinese Academy of Sciences Grant KGZD-EW-303.

1. Rogers JA, Someya T, Huang YG (2010) Materials and mechanics for stretchable electronics. *Science* 327(5973):1603–1607.
2. Nishide H, Oyaizu K (2008) Materials science. Toward flexible batteries. *Science* 319 (5864):737–738.
3. Tarascon JM, Armand M (2001) Issues and challenges facing rechargeable lithium batteries. *Nature* 414(6861):359–367.
4. Kang B, Ceder G (2009) Battery materials for ultrafast charging and discharging. *Nature* 458(7235):190–193.
5. Zhang HG, Yu XD, Braun PV (2011) Three-dimensional bicontinuous ultrafast-charge and -discharge bulk battery electrodes. *Nat Nanotechnol* 6(5):277–281.
6. Pushparaj VL, et al. (2007) Flexible energy storage devices based on nanocomposite paper. *Proc Natl Acad Sci USA* 104(34):13574–13577.
7. Amatucci GG, Badway F, Du Pasquier A, Zheng T (2001) An asymmetric hybrid nonaqueous energy storage cell. *J Electrochem Soc* 148:A930–A939.
8. Nam KT, et al. (2006) Virus-enabled synthesis and assembly of nanowires for lithium ion battery electrodes. *Science* 312(5775):885–888.
9. Liu B, et al. (2012) Hierarchical three-dimensional $ZnCo_2O_4$ nanowire arrays/carbon cloth anodes for a novel class of high-performance flexible lithium-ion batteries. *Nano Lett* 12(6):3005–3011.
10. Jia XL, et al. (2011) Direct growth of flexible $LiMn_2O_4$/CNT lithium-ion cathodes. *Chem Commun* 47(34):9669–9671.
11. Hu LB, Wu H, La Mantia F, Yang Y, Cui Y (2010) Thin, flexible secondary Li-ion paper batteries. *ACS Nano* 4(10):5843–5848.
12. Lima MD, et al. (2011) Biscrolling nanotube sheets and functional guests into yarns. *Science* 331(6013):51–55.
13. Gwon H, et al. (2011) Flexible energy storage devices based on graphene paper. *Energy Environ Sci* 4:1277–1283.
14. Taberna PL, Mitra S, Poizot P, Simon P, Tarascon JM (2006) High rate capabilities Fe_3O_4-based Cu nano-architectured electrodes for lithium-ion battery applications. *Nat Mater* 5(7):567–573.
15. Kang KS, Meng YS, Bréger J, Grey CP, Ceder G (2006) Electrodes with high power and high capacity for rechargeable lithium batteries. *Science* 311(5763):977–980.
16. Aricò AS, Bruce P, Scrosati B, Tarascon JM, van Schalkwijk W (2005) Nanostructured materials for advanced energy conversion and storage devices. *Nat Mater* 4(5): 366–377.
17. Lee S, Cho Y, Song H-K, Lee KT, Cho J (2012) Carbon-coated single-crystal $LiMn_2O_4$ nanoparticle clusters as cathode material for high-energy and high-power lithium-ion batteries. *Angew Chem Int Ed* 124:8878–8882.
18. Feckl JM, Fominykh K, Döblinger M, Fattakhova-Rohlfing D, Bein T (2012) Nanoscale porous framework of lithium titanate for ultrafast lithium insertion. *Angew Chem Int Ed Engl* 51(30):7459–7463.
19. Chen ZP, et al. (2011) Three-dimensional flexible and conductive interconnected graphene networks grown by chemical vapour deposition. *Nat Mater* 10(6):424–428.
20. Nelson PA, Owen JR (2003) A high-performance supercapacitor/battery hybrid incorporating templated mesoporous electrodes. *J Electrochem Soc* 150:A1313–A1317.
21. Aldon L, et al. (2004) Chemical and electrochemical Li-insertion into the $Li_4Ti_5O_{12}$ spinel. *Chem Mater* 16:5721–5725.
22. Lee YJ, et al. (2009) Fabricating genetically engineered high-power lithium-ion batteries using multiple virus genes. *Science* 324(5930):1051–1055.
23. Luo JY, Xia YY (2007) Aqueous lithium-ion battery $LiTi_2(PO_4)_3$/$LiMn_2O_4$ with high power and energy densities as well as superior cycling stability. *Adv Funct Mater* 17: 3877–3884.
24. Lee SW, et al. (2010) High-power lithium batteries from functionalized carbon-nanotube electrodes. *Nat Nanotechnol* 5(7):531–537.
25. Shin JY, Samuelis D, Maier J (2011) Sustained lithium-storage performance of hierarchical, nanoporous anatase TiO_2 at high rates: emphasis on interfacial storage phenomena. *Adv Funct Mater* 21:3464–3472.
26. Ergang NS, et al. (2006) Photonic crystal structures as a basis for a three-dimensionally interpenetrating electrochemical-cell system. *Adv Mater* 18:1750–1753.
27. Ding Y, et al. (2010) Preparation of nano-structured $LiFePO_4$/graphene composites by co-precipitation method. *Electrochem Commun* 12:10–13.
28. Zhou XF, Wang F, Zhu YM, Liu ZP (2011) Graphene modified $LiFePO_4$ cathode materials for high power lithium ion batteries. *J Mater Chem* 21:3353–3358.
29. Tang Y, Huang F, Bi H, Liu Z, Wan D (2012) Highly conductive three-dimensional graphene for enhancing the rate performance of $LiFePO_4$ cathode. *J Power Sources* 203:130–134.
30. Jung HG, Jang MW, Hassoun J, Sun YK, Scrosati B (2011) A high-rate long-life $Li_4Ti_5O_{12}$/$Li[Ni_{0.45}Co_{0.1}Mn_{1.45}]O_4$ lithium-ion battery. *Nat Commun* 2:516–520.
31. Hassoun J, Lee KS, Sun YK, Scrosati B (2011) An advanced lithium ion battery based on high performance electrode materials. *J Am Chem Soc* 133(9):3139–3143.
32. Zhu GN, et al. (2011) Carbon-coated nano-sized $Li_4Ti_5O_{12}$ nanoporous micro-sphere as anode material for high-rate lithium-ion batteries. *Energy Environ Sci* 4:4016–4022.
33. Sun CW, Rajasekhara S, Goodenough JB, Zhou F (2011) Monodisperse porous $LiFePO_4$ microspheres for a high power Li-ion battery cathode. *J Am Chem Soc* 133(7): 2132–2135.